

Vinyl-Terminated Liquid-Crystalline Dendrimers Based on Dendritic Polyols and Their Siloxane-Based Elastomers

Yuteng Lin, Jianzhong Sun

State Key Laboratory of Chemical Engineering, Department of Chemical and Biological Engineering, Zhejiang University, Hangzhou 310027, China
Correspondence to: J. Sun (E-mail: bigwig@zju.edu.cn)

Received 5 July 2012; accepted 1 September 2012; published online 28 September 2012

DOI: 10.1002/pola.26373

ABSTRACT: A new series of side-chain liquid-crystalline dendrimers (LCDs) by grafting vinyl-terminated phenyl benzoate-based promesogens to a novel polypropyleneimine-derived dendritic polyols are reported. Polarized optical microscopy and X-ray diffraction studies show that both the compounds display a smectic-A (SmA) mesophase. The second-generation dendrimer bearing eight-branched promesogens exhibits a more stable SmA mesophase with a wide mesomorphic temperature range. It is demonstrated that “promoting groups” in the structure of LCD for the enhancement of mesomorphic stability are unnecessary in the case of strong anisotropic interactions. In contrast to conventional LCDs, these two compounds possess reactive vinyl terminals that endow them with the potential for the preparation of polymeric materials. For the first time, a type of thermoset elastomers

is explored from LCDs via hydrosilylation crosslinking reaction of vinyl terminals and siloxane crosslinker. Two-dimensional X-ray diffraction study indicates that the lamellar structures of original dendrimers are reserved in the elastomer networks. Stress–strain curves reveal that these elastomers exhibit excellent elasticity under successive uniaxial compression. The combination of anisotropic structures of rigid units and elasticity of flexible networks in this novel series of elastomers makes them promising candidates for the application in artificial muscles or cartilages. © 2012 Wiley Periodicals, Inc. *J Polym Sci Part A: Polym Chem* 51: 71–83, 2013

KEYWORDS: dendrimers; liquid crystal; crosslinking; siloxane; elastomers

INTRODUCTION Dendrimers, as a fascinating class of macromolecular family, have intrigued a great deal of interest of scientists in various areas. In contrast to random hyperbranched polymers, dendrimers possess a perfectly defined core–shell molecular architecture consisting of a multivalent core surrounded by repetitive branching cell units that attached definite number of functional peripheries.¹ These three components are assembled via divergent method or convergent method, and both these methods require an iterative sequence of activation and coupling steps.^{2–4} The hierarchical assembly synthetic strategies of dendrimers endow them with precisely controlled molecular size and shape, monodispersity, absence of chain entanglements, and exponential growth of terminal functional groups. Owing to the spectacular features, dendrimers are potentially promising for versatile applications such as unimolecular container, catalyst support, chiral recognition, light-harvesting antenna, and drug or gene delivery.^{5–9}

The combination of dendrimers with certain fragments at the periphery or in the interior provides the possibility to obtain functional assembles and overall modified macroscopic packing. Dendrimers are able to self-organize into

different types of liquid-crystalline phases by the incorporation of anisometric mesogenic groups. Mesophases of these liquid-crystalline dendrimers (LCDs)^{10–13} result from the molecular arrangement at supramolecular level, which is determined by both the enthalpic gain provided by anisotropic interactions of the mesogenic units and the microphase segregation of two chemically incompatible molecular regions (flexible dendritic core and terminal mesogenic units). Percec and Kawasumi¹⁴ described the first LCD derived from incorporating mesogenic units within a hyperbranched polymer that yielded a nematic phase. With the introduction of the perfect dendritic architecture, various mesophases including smectic phase, hexagonal (Col_h), and rectangular (Col_r) columnar phase have been observed^{15–20} in these monodispersed LCDs. Among LCDs, side-chain LCDs (SC-LCDs) are the most commonly studied. In this approach, mesogenic or promesogenic units are terminally (end-on) or laterally (side-on) attached to the periphery of the preformed dendrimer [polypropyleneimine (PPI), polyamidoamine (PAMAM), polysiloxane, polycarbosilane, and polycarbosilazane]. Terminally attached SC-LCDs exhibit smectic phase commonly, whereas nematic phases are discovered in

most cases of side-on SC-LCDs.^{21,22} Increasing the generation number or number of terminal alkyl chains linked to the mesogenic units can give rise to a columnar mesophase due to self-assembly of disk-like arrangement.^{23–27} If the branching cells are anisometric segments other than long flexible chains, the main-chain LCDs will be obtained. Representative examples of this group is octopus LCDs. Because of the hierarchic incorporation of anisotropic moieties in dendritic branches, the dendrimers favor a regular anisotropic order inducing by a gain in enthalpy. The octopus LCDs show the capability of exhibiting Col_h mesophase when they bear more than one terminal chains, analogous to structure–organization relationship in SC-LCDs.^{28–30} Moreover, besides the 2D-typed mesophase, molecular engineering of LCDs can also give birth to some complicated types of 3D-stacking mesophases such as micellar cubic phase (Cub_I), tetragonal P4₂/mmm phase, and liquid quasicrystal phase.^{31,32}

Although the formation of mesophases of LCDs was induced by the anisotropic interactions and microphase segregation, some “promoting groups” (usually heteroatom-containing groups) that promote but not induce the anisotropic interaction of liquid crystal units or the phase segregation were usually incorporated into the backbones of the dendrimers to enhance the stability of the mesophases. Imino^{21–27} and amide^{28–30,33} groups were commonly seen in the dendritic part of LCDs. The formation of intramolecular and intermolecular hydrogen bonds between these groups helped to maintain a stable aggregation of the dendritic structure, which played a crucial role in the mesogenic behaviors. Furthermore, heteroatom-containing terminals such as fluorinated^{34–38} and cyano^{15,16,39,40} groups would promote the formation of mesophases. The phase-segregation power of fluorinated terminal chains was confirmed to stabilize the liquid-crystalline state. As for the cyano groups, their large dipole moment enable the mesogenic units to preferentially orient into an antiparallel structure and therefore enhance the anisotropic interactions.

As mentioned above, the study of LCDs always focused on the structure–mesomorphism relationship. LCDs with novel molecular structures and exotic mesophases come to the fore successively. Nevertheless, considering the particular three-component molecular structure (dendritic core, mesogenic segment, and terminal chains) of LCDs, two fundamental questions arise:

1. If no chemical group (such as amide and fluorinated group) that will promote the formation of mesophases exists in the dendritic core or at the terminals, then can the dendrimer still display a mesophase? What is the type of the mesophase and what about its stability?
2. As a type of molecules owning unique anisotropic molecular packing, can LCDs be used to prepare polymeric materials such as thermoplastics, thermosets, or elastomers? Will these materials derived from LCDs present any special properties?

Until recently, no detailed study with respect to the mentioned issues has been performed. Concerning the first

question, there is still a need to design new LCDs that avoid the existence of the promoting groups such as imino, amide, fluorinated, and cyano groups. With this in mind, the introduction of stable ester linkages and alkyl terminal chains may be good choice. As for the second question, materials from liquid crystal molecules such as liquid crystal elastomers have been shown to give intriguing properties. Liquid crystal elastomers, derived from linear liquid crystal monomers, have become an attractive class of liquid crystal materials. The novel macroscopic feature of combining elasticity of polymer networks and anisotropic structure of liquid-crystalline phases offered liquid crystal elastomers the possibility of application in artificial muscles and active smart surfaces.^{41–49} Accordingly, we were interested in transferring the concept of liquid crystal elastomers to LCDs by preparing elastomers via LCDs owning more perfect anisotropic structures but not randomly formed liquid-crystalline dendritic network.⁵⁰ To open up the possibility, the terminals of the LCDs should be modified with reactive groups such as crosslinkable vinyl group,⁵¹ curable epoxide group,⁵² and photopolymerizable acrylate group,⁵³ other than the conventional nonreactive groups (saturated alkyl, fluorinated, and cyano groups). Taking into consideration the concerns of the two issues above simultaneously, a series of new LCDs consisting of dendritic part with ester linkages, mesogenic units, and unsaturated alkyl chains (vinyl terminals) will be exploited.

Therefore, in this work, we first designed a benzoate-type promesogen with a reactive vinyl terminal. Second, a novel type of dendritic polyols, **G1-(OH)₄** and **G2-(OH)₈**, owning hydroxyl peripheries other than amine peripheries of PPI or PAMAM, were synthesized according to a two-step procedure. As a consequence of the attachment of these polyols with vinyl-terminated promesogens using a stable covalent ester linkage, which was rarely reported in SC-LCDs,^{54–57} side-chain dendrimers **G1-(MU)₄** and **G2-(MU)₈** bearing four or eight promesogenic units were obtained without incorporation of any promoting group. The mesogenic behaviors of these two dendrimers were then investigated by a combination of analytical techniques such as differential scanning calorimeter (DSC), polarized optical microscope (POM), and X-ray diffraction (XRD). Moreover, the reactive vinyl terminals of this series of LCDs endowed them with the possibility of further evolution toward polymeric materials. Considering the characteristics of the vinyl terminals, a classic technique of siloxane–vinyl hydrosilylation reaction that was most commonly used in the preparation of liquid crystal elastomers^{41–44,46–49} was applied. The crosslinking reaction of siloxane crosslinker with the terminal vinyl bonds of **G1-(MU)₄** or **G2-(MU)₈** yielded a novel type of thermoset elastomers, in which the molecular packing of original LCDs was observed to maintain in the network of elastomers. During successive uniaxial compression experiments, the stress–strain curves revealed that these elastomers exhibited excellent elasticity that indicated the combination of anisotropic structures of rigid units and elasticity of flexible networks in this series of elastomers.

EXPERIMENTAL

Materials

10-Undecen-1-ol, 4-hydroxybenzaldehyde, *N,N'*-dicyclohexylcarbodiimide (DCC), 4-dimethylaminopyridine (DMAP), sodium chlorite, and 1,4-diaminobutane were purchased from Acros and used as received. *p*-Toluenesulfonyl chloride (TsCl), methyl 4-hydroxybenzoate, *tert*-butyl acrylate, LiAlH₄, and resorcinol (from TCI) were used as received. Polypropyleneimine tetramine dendrimer (first generation, DAB-Am-4) and platinum(0)-1,3-divinyl-1,1,3,3-tetramethyldisiloxane [Pt(dvs)] complex solution (in xylene, 2%) was purchased from Aldrich. Tetrakis(dimethylsiloxy)silane (TDS) was purchased from Alfa Aesar. Pyridine, CH₂Cl₂, THF, and toluene were purified according to standard protocols. Resorcinol, *tert*-butanol, acetone, NaOH, K₂CO₃, NaH₂PO₄·2H₂O, MgSO₄, Na₂SO₄, hydrochloric acid (37 wt % aqueous solution), MeOH, EtOH, and Et₂O were used as received.

Synthesis of Promesogen

Compound **3** was synthesized via a three-step technique according to a literature procedure.⁵⁸

4-Formylphenyl 4-(undec-10-en-1-yloxy)benzoate (**4**)

Compound **3** (1 g, 3.45 mmol), 4-hydroxybenzaldehyde (0.421 g, 3.45 mmol), and DMAP (0.005 g, 0.04 mmol) were dissolved in CH₂Cl₂ (20 mL) under argon atmosphere. After addition of DCC (1.06 g, 5.14 mmol), the mixture was stirred at 25 °C for 48 h under Ar atmosphere. On completion of the reaction, the reaction mixture was filtered, and then the filtrate was washed with H₂O (15 mL) for three times. The organic layer was dried over anhydrous Na₂SO₄. The solvent was evaporated under vacuum. The resulted yellow solid was purified by column chromatography (silica gel) with CH₂Cl₂ as the eluting solvent to give a white solid (1.01 g, 74% yield).

¹H NMR (CDCl₃): δ = 10.03 (s, 1H), 8.16 (d, 2H), 7.99 (d, 2H), 7.40 (d, 2H), 7.01 (d, 2H), 5.78 (m, 1H), 4.96 (m, 2H), 4.06 (t, 2H), 2.07 (m, 2H), 1.84 (m, 2H), 1.49–1.32 ppm (overlapped peaks, m, 12 H). ¹³C NMR (CDCl₃): δ = 190.82, 164.11, 163.79, 155.84, 139.06, 133.81, 132.32, 131.10, 122.49, 120.75, 114.35, 114.05, 68.30, 33.67, 29.36, 29.29, 29.21, 28.97, 28.81, 25.85 ppm.

4-((4-(Undec-10-en-1-yloxy)benzoyl)oxy)benzoic acid (**5**)

To a solution of Compound **4** (0.611 g, 1.55 mmol) and resorcinol (0.22 g, 2 mmol) in *tert*-butanol (30 mL), sodium chlorite (0.81 g, 8.96 mmol) and NaH₂PO₄·2H₂O (0.725 g, 4.65 mmol) in H₂O (8.5 mL) was added slowly within 20 min under Ar atmosphere. The mixture was stirred at 30 °C for 48 h. The progress of reaction was monitored by thin layer chromatography (TLC) (CH₂Cl₂). After *tert*-butanol was evaporated, the mixture was diluted with H₂O (50 mL) and neutralized with aqueous HCl (1 mol/L). The formed precipitate was filtered and washed with plenty of water. Purification by column chromatography (silica gel, CH₂Cl₂) gave the product as a white solid (0.575 g, 90% yield).

¹H NMR (DMSO-*d*₆): δ = 13.03 (s, 1H), 8.05 (m, 4H), 7.39 (d, 2H), 7.09 (d, 2H), 5.77 (m, 1H), 4.93 (m, 2H), 4.06 (t, 2H),

1.99 (m, 2H), 1.73 (m, 2H), 1.40–1.26 ppm (overlapped peaks, m, 12 H). ¹³C NMR (DMSO-*d*₆): δ = 166.99, 164.16, 163.73, 154.56, 139.17, 132.48, 131.24, 128.69, 122.53, 120.77, 115.06, 114.96, 68.36, 33.54, 29.31, 29.17, 29.08, 28.87, 28.64, 25.76 ppm. Electrospray ionization-mass spectrometry (ESI-MS): *m/z*: 409.2 [M-H]⁺.

Synthesis of Dendritic Core with Hydroxyl Periphery

Tetra-tert-butyl 3,3',3'',3'''-(butane-1,4-diylbis(azanetriyl))tetrapropanoate (6)

Tert-butyl acrylate (6.5 mL, 44.6 mmol) was added dropwise to a solution of 1,4-diaminobutane (0.758 g, 8.60 mmol) in MeOH (10 mL) under Ar atmosphere. The reaction mixture was stirred for 24 h at room temperature. The volatiles of the mixture were evaporated under vacuum to afford a yellow viscous liquid (4.14 g, 80% yield).

¹H NMR (CDCl₃): δ = 2.71 (t, 8H), 2.39–2.32 (overlapped peaks, m, 12H), 1.44–1.40 ppm (overlapped peaks, m, 40H). ¹³C NMR (CDCl₃): δ = 171.98, 80.07, 53.47, 49.14, 33.55, 27.98, 24.96 ppm. ESI-MS: *m/z*: 601.4 [M+H]⁺.

3,3',3'',3'''-(Butane-1,4-diylbis(azanetriyl))tetrakis(propan-1-ol) [G1-(OH)]₄

A solution of Compound **6** (3.02 g, 5.03 mmol) in anhydrous THF (15 mL) was added to a suspension of LiAlH₄ (1.07 g, 28.2 mmol) in anhydrous THF (20 mL) in an ice bath under Ar atmosphere. After stirring in the ice bath, the mixture was warmed to room temperature and stirred for another 2 h. To quench the reaction, ice water (1 g), 15% aqueous NaOH (3 g), and ice water (1 g) were added sequentially to the reaction mixture. The resulting mixture was dried with anhydrous MgSO₄ and filtered. The filtrate was concentrated under vacuum to give a yellow viscous liquid (1.37 g, 85% yield).

¹H NMR (CDCl₃): δ = 4.71 (s, 4H), 3.65 (t, 8H), 2.54 (t, 8H), 2.39 (s, 4H), 1.65 (m, 8H), 1.45 ppm (s, 4H). ¹³C NMR (CDCl₃): δ = 62.07, 53.73, 52.70, 28.43, 24.76 ppm. ESI-MS: *m/z*: 321.4 [M+H]⁺, 161.2 [M+2H]²⁺.

Di-tert-butyl 8,13-bis(3-(bis(3-(tert-butoxy)-3-oxopropyl)amino)propyl)-4,17-bis(3-(tert-butoxy)-3-oxopropyl)-4,8,13,17-tetraazaicosane-1,20-dioate (7)

Compound **7** was synthesized by the same general procedure as the synthesis of Compound **6**. Starting from DAB-Am-4 (0.15 g, 0.474 mmol) in MeOH (3 mL) and *tert*-butyl acrylate (0.76 mL, 5.22 mmol), 0.572 g (90% yield) of Compound **7** was obtained as a yellow viscous liquid.

¹H NMR (CDCl₃): δ = 2.72 (t, 16H), 2.41–2.32 (overlapped peaks, m, 36H), 1.55 (m, 8H), 1.43–1.37 ppm (overlapped peaks, m, 76H). ¹³C NMR (CDCl₃): δ = 172.07, 80.06, 54.06, 51.90, 51.83, 49.12, 33.49, 28.01, 24.87, 24.70 ppm. ESI-MS: *m/z*: 1342.6 [M+H]⁺.

8,13-Bis(3-(bis(3-hydroxypropyl)amino)propyl)-4,17-bis(3-hydroxypropyl)-4,8,13,17-tetraazaicosane-1,20-diol [G2-(OH)]₈

A synthetic procedure analogous to the one described in the synthesis of **G1-(OH)₄** was used. The reaction of Compound **7** (0.369 g, 0.275 mmol) in THF (5 mL) and LiAlH₄ (0.117 g,

3.08 mmol) in THF (10 mL) afforded **G2-(OH)₈** as a yellow viscous liquid (0.185 g, 86% yield).

¹H NMR (CDCl₃): δ = 4.93 (s, 8H), 3.64 (t, 16H), 2.55 (t, 16H), 2.43–2.35 (overlapped peaks, m, 20H), 1.67–1.56 (overlapped peaks, m, 24H), 1.38 ppm (m, 4H). ¹³C NMR (CDCl₃): δ = 62.06, 54.10, 52.73, 52.06, 51.93, 28.59, 24.99, 24.28 ppm. ESI-MS: *m/z*: 804.1 [M+Na]⁺, 781.7 [M+H]⁺, 391.3 [M+2H]²⁺.

Esterification of Mesogenic Unit with Dendritic Core

Synthesis of **G1-(MU)₄**

Compound **G1-(OH)₄** (0.192 g, 0.6 mmol), Compound **5** (1.18 g, 2.87 mmol), and DMAP (0.0351 g, 0.288 mmol) were dissolved in CH₂Cl₂ (50 mL) in an ice bath under Ar atmosphere. A solution of DCC (0.712 g, 3.45 mmol) in CH₂Cl₂ (20 mL) was then added dropwise. The reaction mixture was stirred at room temperature for 2 days. H₂O (0.6 mL) was added to the mixture and the precipitate was filtered. The filtrate was concentrated under vacuum, and the resulting solid was washed with plenty of hot hexane. The yellow crude product was further purified by column chromatography (silica gel, CH₂Cl₂/MeOH, from 40:1 to 30:1) followed by a recrystallization in acetone to give a yellow solid (0.454 g, 40% yield).

¹H NMR (CDCl₃): δ = 8.11 (m, 16H), 7.28 (d, 8H), 6.95 (d, 8H), 5.82 (m, 4H), 4.96 (m, 8H), 4.40 (t, 8H), 4.04 (t, 8H) 2.62 (s, 8H), 2.46 (s, 4H), 2.05 (m, 8H), 1.93 (s, 8H), 1.83 (m, 8H), 1.49–1.32 ppm (overlapped peaks, m, 52H). ¹³C NMR (CDCl₃): δ = 165.71, 164.21, 163.61, 154.68, 139.07, 132.25, 130.97, 127.68, 121.72, 121.00, 114.26, 114.05, 68.24, 63.25, 53.93, 50.32, 33.68, 29.59, 29.37, 29.30, 29.24, 28.99, 28.81, 26.60, 25.87 ppm. MALDI-TOF MS: *m/z*: 1891.3 [M+H]⁺.

Synthesis of **G2-(MU)₈**

Compound **G2-(MU)₈** was synthesized by using a similar procedure as the synthesis of **G1-(MU)₄**. The reagents used were **G2-(OH)₈** (0.156 g, 0.2 mmol), Compound **5** (0.788 g, 1.92 mmol), DMAP (0.0234 g, 0.192 mmol) in CH₂Cl₂ (25 mL), and DCC (0.475 g, 2.3 mmol) in CH₂Cl₂ (3 mL). In this case, longer reaction time (5 days) was necessary for complete esterification of hydroxyl group of **G2-(OH)₈**. Purification by column chromatography (silica gel, CH₂Cl₂/MeOH, from 30:1 to 16:1) followed by a recrystallization in acetone afforded **G2-(MU)₈** as a yellow solid (0.235 g, 30% yield).

¹H NMR (CDCl₃): δ = 8.08 (m, 32H), 7.26 (d, 16H), 6.93 (d, 16H), 5.84 (m, 8H), 4.99 (m, 16H), 4.36 (s, 16H), 4.01 (m, 16H), 2.60 (m, 16H), 2.45 (m, 20H), 2.05 (m, 16H), 1.91 (m, 16H), 1.82 (m, 16H), 1.61 (m, 8H), 1.48–1.32 ppm (overlapped peaks, m, 100H). ¹³C NMR (CDCl₃): δ = 165.66, 164.18, 163.53, 154.60, 139.09, 132.23, 130.96, 127.46, 121.76, 120.86, 114.18, 114.05, 68.13, 63.22, 61.27, 53.07, 52.44, 49.98, 33.70, 29.60, 29.39, 29.31, 29.25, 29.00, 28.79, 26.14, 25.85 ppm. MALDI-TOF MS: *m/z*: 3922.2 [M+H]⁺.

Preparation of Elastomers

In a 2-mL tube with an inner diameter of 5 mm, **G1-(MU)₄** (0.0984 g, 0.05 mmol) or **G1-(MU)₈** (0.098 g, 0.025 mmol) and TDS (18.6 μL, 0.05 mmol) were dissolved in 0.3 mL of

dry toluene. Then, 10 μL of Pt(dvs) (2 wt % in xylene) was added, and then the tube was sealed with a cap. The reaction mixture was heated at 50 °C for 2 days. Afterward, the formed elastomers were carefully removed from the tubes. The residual solvent was allowed to evaporate slowly at room temperature to obtain dry elastomers. To evaluate the formation process of the elastomers under different ratio of vinyl group to Si–H bond, the amount of TDS added into the reaction mixture was reduced to 9.8 μL (0.025 mmol) or 4.9 μL (0.0125 mmol).

Characterization

¹H NMR and ¹³C NMR were recorded on a Bruker DRX-400 (400 MHz) instrument with CDCl₃ or DMSO-*d*₆ as the solvent (with tetramethylsilane as an internal standard). MALDI-TOF mass spectra were performed using a microflex mass spectrometer (Bruker Daltonics) with α-cyano-4-hydroxycinnamic acid as a matrix. The ESI-MS analyses were measured on a Bruker Esquire-LC-00075 spectrometer. Thermal transitions were detected on a TA Instruments 200 DSC at a scanning rate of 10 °C/min in all cases. First-order transitions were reported as the maxima and minima of the endothermic and exothermic peaks. A POM (Nikon LV100 POL) coupled with a Linkam MDS600 hot stage was used to observe the anisotropic textures and to verify thermal transitions.

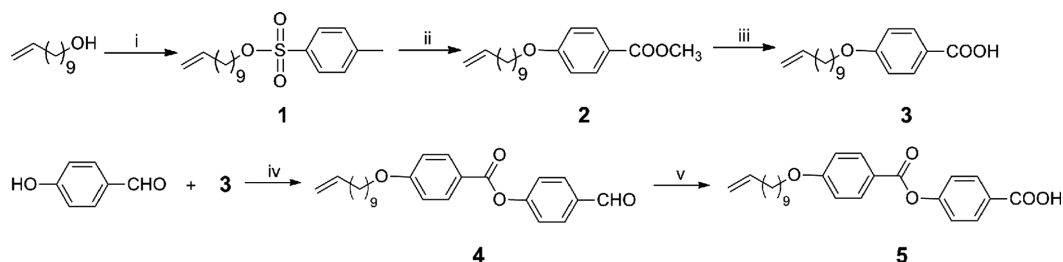
The XRD experiments were recorded by synchrotron radiation XRD at beamline BL14B1, provided by the Shanghai Synchrotron Radiation Facility, at a wavelength of 0.68873 Å. BL14B1 is a beamline based on bending magnet, and a Si (111) double-crystal monochromator was used to monochromatize the beam. The size of the focus spot is about 0.5 mm, and the end station is equipped with a Huber 5021 diffractometer. NaI scintillation detector was used for data collection. The powder samples were cast from THF solution and then mounted on the sample stage. A temperature control unit (Mettler hot stage FP82HT) in conjunction with the diffractometer was used to study the structural evolutions as a function of temperature. Moreover, a MAR345 image detector was used to record two-dimensional (2D) X-ray patterns of the elastomers. The powder rings were integrated with the FIT2D code.

Cyclic compression experiments were carried out on a Zwick/Roell Z020 universal testing machine equipped with a 25-kN load cell. The elastomer was in the form of a cylinder (~5 mm diameter and 4 mm in initial thickness). In a typical compressive cycle, the test began with a compression step performed at a constant crosshead speed of 0.3 mm/min to a final strain of 50%, followed by immediate retraction to zero load and a wait time, ~1 min, until the next cycle of compression. Stress-strain data were collected during the compression process.

RESULTS AND DISCUSSION

Synthesis of Promesogen, Dendritic Polyols, and Dendrimers

The synthetic procedure used to obtain promesogen **5** is outlined in Scheme 1. The benzoate-type mesogenic segment was accomplished by direct room-temperature DCC-



SCHEME 1 Synthetic route of the terminally attached mesogenic unit: (i) TsCl, pyridine; (ii) methyl 4-hydroxybenzoate, K_2CO_3 , acetone; (iii) KOH, EtOH/ H_2O ; (iv) DCC, DMAP, CH_2Cl_2 ; and (v) sodium chlorite, NaH_2PO_4 , *tert*-butanol.

promoted esterification of 4-(undec-10-en-1-yloxy)benzoic acid (**3**) and methyl 4-hydroxybenzoate.⁵⁹ Subsequent oxidation of aldehyde group to afford the corresponding acid was achieved according to an analogous method described previously.⁶⁰ As shown in 1H NMR (Fig. 1), the disappearance of chemical shift of aldehyde group ($\delta = 10.03$ ppm) and emerging shift of benzoic acid ($\delta = 13.03$ ppm) indicated the complete oxidation. Moreover, characteristic signals of vinyl group ($CH_2=CH-$) were observed at 5.77 and 4.93 ppm. The integration ratio of all the signals agreed with the calculated value, which confirmed the exact structure of Compound **5**.

Dendritic polyols were prepared by a two-step synthetic technique (Scheme 2). First, Michael addition of *tert*-butyl acrylate with 1,4-diaminobutane or PPI (a commercial dendrimer) gave rise to a series of dendrimers with *tert*-butyl ester termination. Subsequently, the reduction of the terminated *tert*-butyl ester groups with $LiAlH_4$ afforded two generations of dendrimers with hydroxyl periphery, which were named as **G1-(OH)₄** and **G2-(OH)₈**, respectively. 1H NMR spectrum of **G2-(OH)₈** [Fig. 2(A)] showed characteristic signal of hydroxyl periphery at $\delta = 4.93$ ppm. The proton signals of all the methylene groups were assigned as indicated in the figure. Molecular mass of **G2-(OH)₈** was determined by ESI-MS technique, exhibiting three peaks for $[M+H]^+$, $[M+2H]^{2+}$, and $[M+Na]^+$ [Fig. 2(B)]. The formation of **G1-(OH)₄** was also confirmed by its 1H NMR and ESI-MS spectra. The spectroscopic data are described in detail in the Experimental section.

The mesogenic functional side-chain dendrimers [**G1-(MU)₄** and **G2-(MU)₈**] were synthesized by esterification of 4-(4-(undec-10-en-1-yloxy)benzoyloxy)benzoic acid (**5**) with the terminal hydroxyl groups of the corresponding generation of dendritic polyols [**G1-(OH)₄** and **G2-(OH)₈**] (Scheme 3). These dendritic compounds show much better solubility than that of promesogen **5** in common solvents such as dichloromethane, chloroform, and THF. The structures of both new dendrimers have been confirmed by 1H NMR, ^{13}C NMR, and MALDI-TOF mass spectrometry. Evidence for the esterification reactions was provided by the existence of a signal at $\delta = 4.4$ ppm in 1H NMR spectra (Fig. 3), which corresponds to the protons of $-CH_2-$ group linked to the ester bond. As shown in 1H NMR spectra, the main difference between **G1-(MU)₄** and **G2-(MU)₈** lies in chemical shift at $\delta = 2.60$, 2.45, and 1.61 ppm due to the various architecture

of dendritic core. Every signal in the spectra was assigned to the corresponding protons of the dendrimers. The ratio of the quantitative signal integration is in good agreement with the prediction. MALDI-TOF mass spectrum (Fig. 4) clearly showed the parent peak at m/z 1891.3 for **G1-(MU)₄** ($[M+H]^+$ calcd. 1891.4) and 3922.2 for **G2-(MU)₈** ($[M+H]^+$ calcd. 3922.1) that also indicated entire substitution at the periphery.

Thermal Transition and Mesomorphic Properties

The phase transition of mesogenic monomers (**4** and **5**) and mesogen-substituted dendrimers [**G1-(MU)₄** and **G2-(MU)₈**] have been studied by DSC, with heating and cooling rates of 10 °C/min. Moreover, the mesomorphic textures were evaluated from polarized optical microscopy. The aldehyde-terminated monomer **4** exhibits a narrow nematic phase below 70 °C, which is characterized by a schlieren texture. However, the promesogen **5** with benzoic group owns a more ordered and stable smectic-A (SmA) phase between 84 and 206 °C. This is attributed to the intermolecular hydrogen bond interactions. Thermal transition and thermodynamic data are summarized in Table 1.

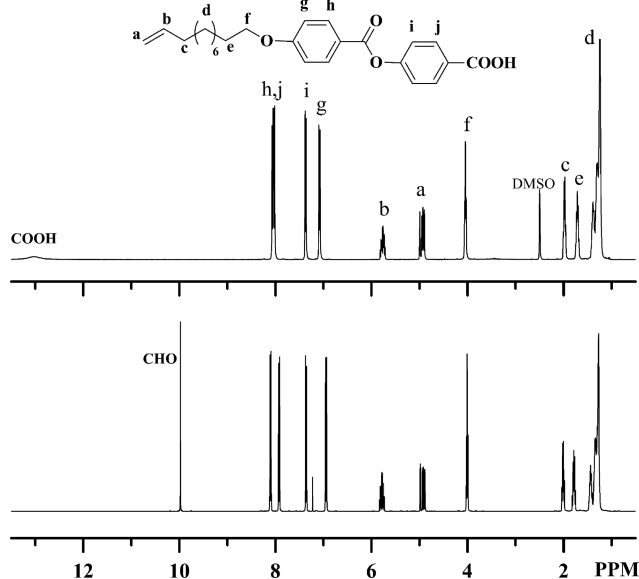
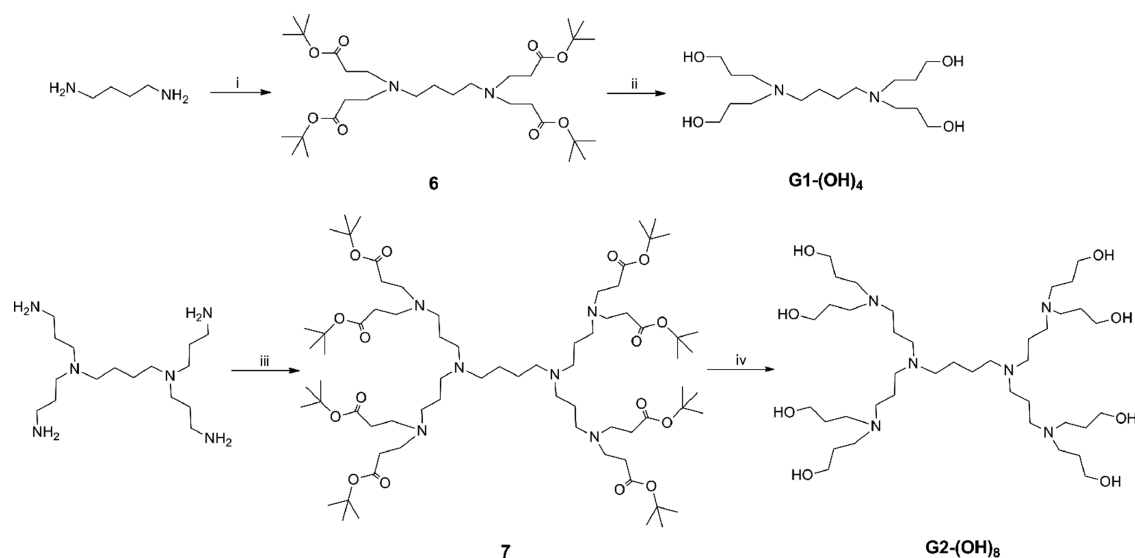


FIGURE 1 1H NMR spectrum of promesogen **5** (upper, $DMSO-d_6$) and compound **4** (lower, $CDCl_3$).



SCHEME 2 Synthetic route of dendritic core with hydroxyl periphery: (i) *tert*-butyl acrylate, MeOH and (ii) LiAlH₄, THF.

The first-generation dendrimer, **G1-(MU)₄**, exhibits simple thermograms in the heating and cooling scan that both consist of two thermal transition peaks [Fig. 5(A)]. In the first cooling scan, one can distinguish an isotropic liquid–mesophase transition at 106 °C and a mesophase–crystallization transition at 92 °C. The characteristic mesophase was confirmed by the optical texture from POM observation. Figure 6(A) shows a typical fan-shaped texture of **G1-(MU)₄** at 100 °C, which is characteristic of a lamellar SmA mesophase. Moreover, a narrow mesomorphic temperature range of 106–92 °C indicates an unstable mesophase of **G1-(MU)₄**. However, with an analogous molecular architecture, the PAMAM dendrimer PAMAM[L]₄ (first generation) displayed a stable SmA mesophase due to the stabilization by intramolecular hydrogen bond by promoting groups (amido groups), which promoted the lamellar packing of mesogens.²⁶

In the case of dendrimer **G2-(MU)₈**, a complex melting behavior was observed according to the second heating of DSC scan [Fig. 5(B)]. On heating, several endotherms and two recrystallization exothermal peaks were visible. The endotherms were ascribed to the melting of various crystalline forms. Those two cold crystallizations (at 29 and 69 °C) resulted from the incomplete ordering of the molecules during cooling. When the DSC thermogram was recorded at a low cooling rate of 1 °C/min, exotherm at 29 °C disappeared, whereas cold crystallization remained at 69 °C. The obvious cold-crystalline behaviors indicated that molecular crystallization of **G2-(MU)₈** was strongly inhibited by its malleable branch topology. This broad melting/recrystallization trajectory during heating process is commonly for dendrimers and dendrons.^{16,61,62} Subsequent heating of **G2-(MU)₈** would lead to a SmA mesophase characterized by a typical fan-shaped texture.

In the cooling scan of **G2-(MU)₈**, a very simple thermogram containing only an isotropic transition ($T_i = 111$ °C) and a crystalline transition ($T_k = 12.6$ °C) identifies a wide range of stability of this mesophase, which is in accordance to the

results of polarized optical microscopy. Figure 6(B) shows the initial formation of a fan-shaped SmA phase at 95 °C on cooling, and the SmA phase maintains at room temperature

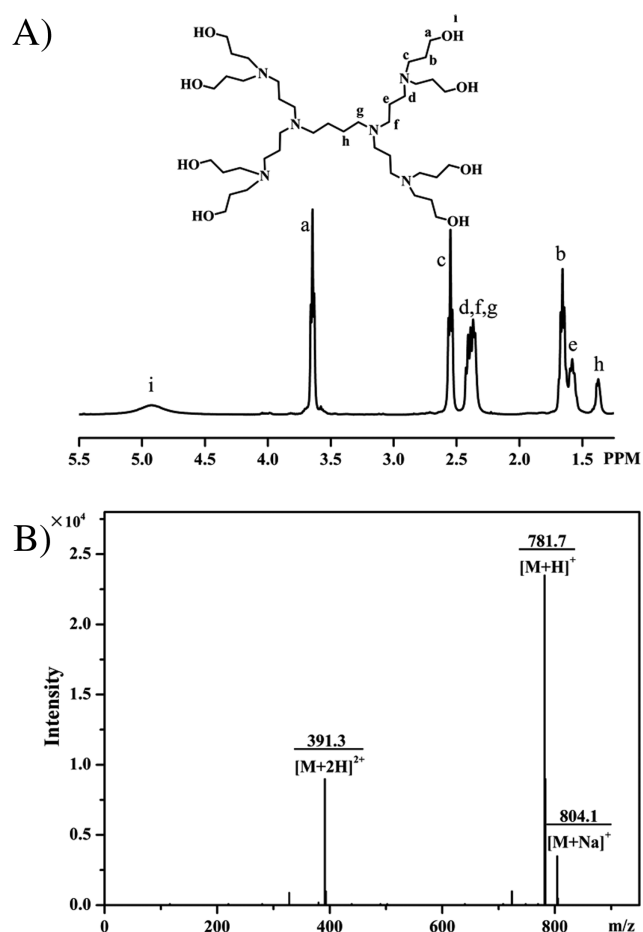
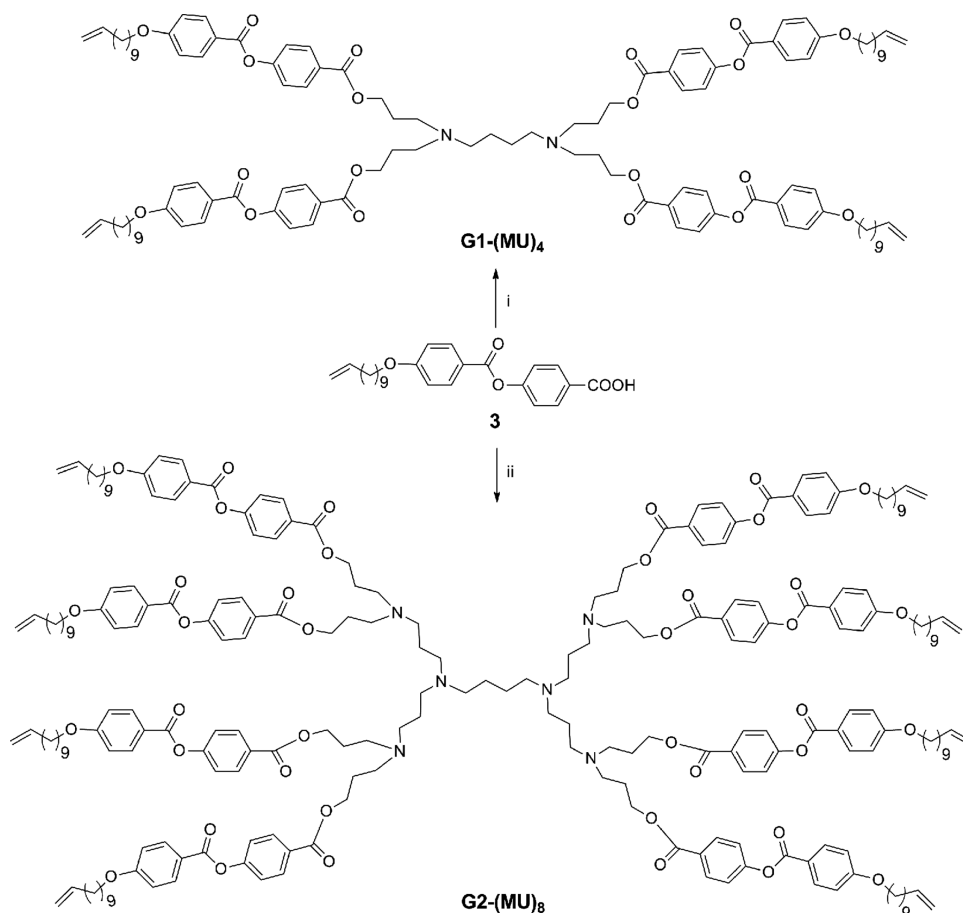


FIGURE 2 ¹H NMR spectrum (A) and ESI-MS spectrum (B) of dendritic core **G2-(OH)₈** with hydroxyl periphery.



SCHEME 3 Synthetic route of dendrimers functionalized with mesogenic units: (i) **G1-(OH)₄**, DCC, DMAP and (ii) **G2-(OH)₈**, DCC, DMAP.

($T = 20\text{ }^{\circ}\text{C}$), which is characterized by the enlarged fan-shaped texture shown in Figure 6(C).

In contrast to **G1-(MU)₄**, increasing mesogenic groups at the peripheries of dendritic core of **G2-(MU)₈** enhanced the anisotropic interactions between them. As a consequence, enthalpy gain provided by strong anisotropic interactions dominated entropy force that leads to an isotropic distribution, therefore resulting in the formation of a stable SmA mesophase with a wide mesomorphic temperature range. Therefore, in this series of LCDs without any promoting group, although driving forces such as hydrogen bond, phase-segregation power, and dipole moments are absent, lamellar mesophases are still displayed. The stronger the anisotropic interactions between mesogenic units are, the more stable the mesophase will exhibit.

Molecular Packing of LCDs

As can be seen from the results presented in Table 1 and Figure 6, **G1-(MU)₄** and **G2-(MU)₈** both show a SmA phase. As SmA phase is typical orientation of elongated molecules, the phase nature of the molecular packing of the two dendrimers is identified by wide-angle X-ray diffraction experiments. For this study, the samples all underwent a thermal treatment consisting of heating to the isotropic state, annealing at this state for 2 min and cooling consequently.

The XRD pattern of **G1-(MU)₄** at $100\text{ }^{\circ}\text{C}$ contains a set of four equidistant sharp peaks in the small-angle region, with the intensity of the reflections decreasing with Bragg angles

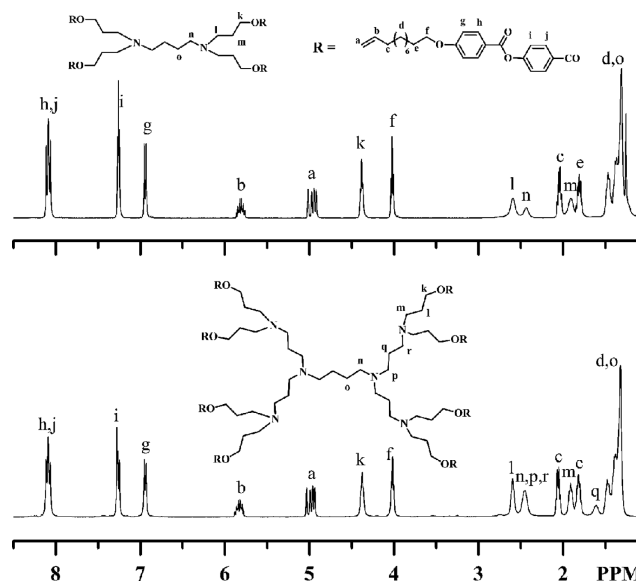


FIGURE 3 ^1H NMR spectrum (CDCl_3) of side-chain dendrimers **G1-(MU)₄** (upper) and **G2-(MU)₈** (lower).

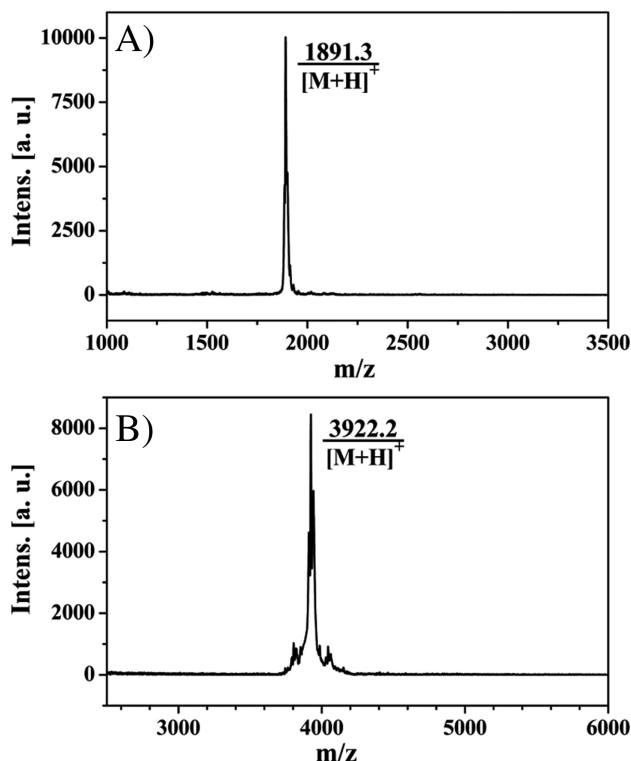


FIGURE 4 MALDI-TOF MS of side-chain dendrimers: (A) **G1-(MU)₄** and (B) **G2-(MU)₈**.

[Fig. 7(A)]. The reciprocal spacing ($q = 4\pi \sin \theta / \lambda$) ratio of 1:2:3:4 for the four diffractions is characteristic of a well-developed lamellar morphology. The maxima correspond to the first-, second-, third-, fourth-order reflections on the lamellar planes, respectively. As for **G2-(MU)₈** at 70 °C, a set of three equidistant sharp peaks with the reciprocal spacing ratio of 1:2:3 shown in Figure 7(B) also indicates a layer packing. These results are consistent with smectic meso-

TABLE 1 Thermal Transitions of Compounds **4**, **5**, **G1-(MU)₄**, and **G2-(MU)₈**^a

Compound	Thermal Transitions (°C) [Corresponding Enthalpy Changes (J/g)]
4	K 56.0 (30.33) N 62.1 (86.17) I I 63.7 (2.57) N 45.2 (110.3) K
5	K 104.6 (32.41) SmA 210.4 (12.03) I I 205.7 (11.06) SmA 86.4 (33.19) K
G1-(MU)₄	K 97.8 (2.68) SmA 122.2 (65.44) I I 106.2 (67.09) SmA 92.5 (1.78) K
G2-(MU)₈	K ₁ 15.9 (3.01) -K 28.8 (12.73) K ₂ 63.2 (16.76) -K 68.9 (12.63) K ₃ 81.5 (15.7) SmA 117.7 (14.45) I I 111.0 (15.82) SmA 12.6 (2.81) K

^a Data from the second heating DSC scan are on the first line, and data from the first cooling scan are on the second line. Phases are indicated as follows: K: crystal phases; SmA: smectic-A phase; N: nematic phase; and I: isotropic phase.

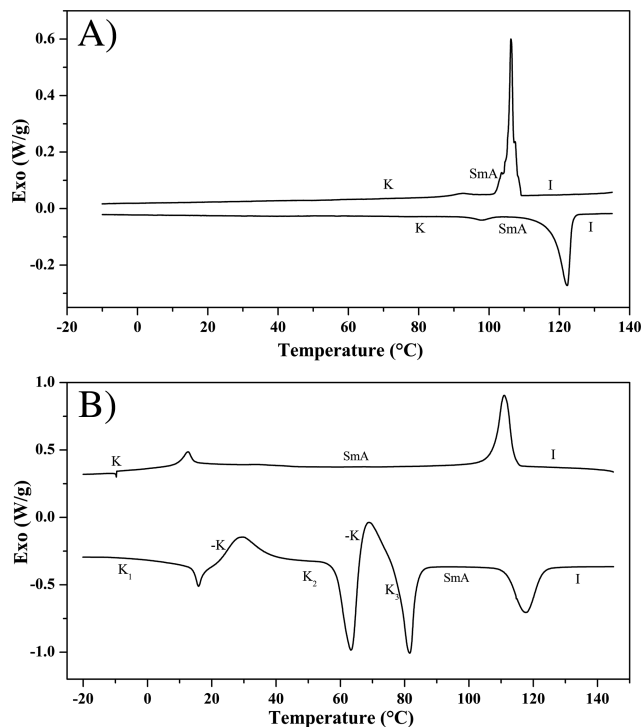


FIGURE 5 Second heating (lower curve) and first cooling (upper curve) DSC traces of dendritic compounds (A) **G1-(MU)₄** and (B) **G2-(MU)₈** at a rate of 10 °C/min. Phases are indicated as follows: K: crystal phases; SmA: smectic-A phase; and I: isotropic phase.

phase, confirming the POM observations. The layer periodicity ($d = 2\pi/q$) of the two dendritic compounds are gathered in Table 2. The proposed molecular organization model of the two dendrimers within the smectic mesophase is represented schematically in Figure 8. The dendritic polyols spacers are conformationally disordered and occupy the central segment of the smectic layers. The mesogenic units necessarily extend up and down from the central dendritic part in a pseudoparallel mode to allow for the formation of lamellar mesophase. As indicated in Table 2, layer thickness (32.9 Å) of **G2-(MU)₈** is larger than that of **G1-(MU)₄** (30.8 Å), which is associated with a preferentially extended conformation of the dendritic core. However, in both cases of **G1-(MU)₄** and **G2-(MU)₈**, the layer spacing is much smaller than the molecular length evaluated from its most extended conformation (calculated by molecular simulations). Two extremely disordered parts, the terminal hydrocarbon chains and the dendritic cores, are responsible for this distinct compression. Dendritic core, the central part of the molecule, tends to adopt a very curled arrangement, and finally it contributes mainly to the molecular width rather than the molecular length.

Elastomers from LCDs

As shown in Scheme 3, LCDs, **G1-(MU)₄** and **G2-(MU)₈**, possess four or eight vinyl groups at their terminals that endow them with the capability of further functionalization. The elastomers derived from the two dendrimers were prepared

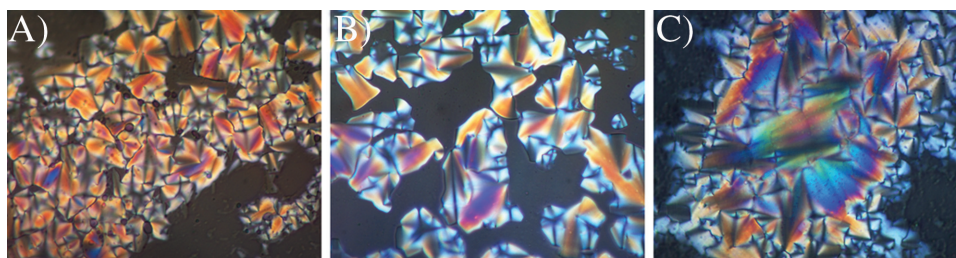


FIGURE 6 Polarized optical microphotographs of the textures of (A) **G1-(MU)₄** at 100 °C on cooling, (B) **G2-(MU)₈** at 95 °C on cooling, and (C) **G2-(MU)₈** at 20 °C on cooling. Both of the heating and cooling rate is 1 °C/min.

following a one-pot hydrosilylation reaction catalyzed by Karstedt's catalyst [Pt(dvs)] and involving the double bonds of the terminals of the dendrimers and the silane groups of the crosslinkers (TDS) with four crosslinking points. A rough 2D schematic representation of the formation of such an elastomer network is shown in Figure 9. The networks consist of rod-like mesogens, flexible dendritic part, and siloxane-based crosslinking area.

In the preparation of elastomers **G1-TDS** and **G2-TDS**, the ratio between vinyl groups and the hydrogen of silane was

stoichiometric. Hydrosilylation reaction was carried out in concentrated toluene solution (0.67 mmol/mL vinyl bonds). The resulting samples were solid and flawless cylinders with a diameter of 5 mm and a height of 4 mm [Fig. 10(A, D)]. Both of the samples were proven to be thermoset elastomers because of their insoluble and infusible characters that indicated highly crosslinked network. Moreover, the ratio of vinyl bond to Si–H bond had a great impact on the crosslinking density of the network, which finally affected the formation of elastomers. A higher ratio of 2:1 would lead to fragile gels with extremely low strength due to the reduced crosslinking density of the resulting network [Fig. 10(B, E)]. Furthermore, in the most weakly crosslinked network (a ratio of 4:1), not a single piece of gel was found in the final reaction solution. If the crosslinker with low connectivity such as tetramethyldisiloxane was used to prepare the elastomers, only small pieces of fragile gels or total solution were obtained, no matter which ratio of vinyl group to Si–H bond and what types of LCDs [**G1-(MU)₄** or **G2-(MU)₈**] were applied.

Although it was impossible to identify the phase behaviors of these thermoset elastomers because of their infusible feature, a lamellar-like scattering pattern was found in structural characterization by 2D XRD recorded at room temperature, as shown in Figure 11(A, B). The corresponding azimuthally integrated XRD patterns (intensity versus scattering vector magnitude q) are presented in Figure 11(C, D). For **G1-TDS** with polydomain, two diffraction arcs located at low angles indicated ordered lamellar structure within the elastomer. The two peaks in the small angle region, which are well fitted by Lorentzian curves, corresponding to the

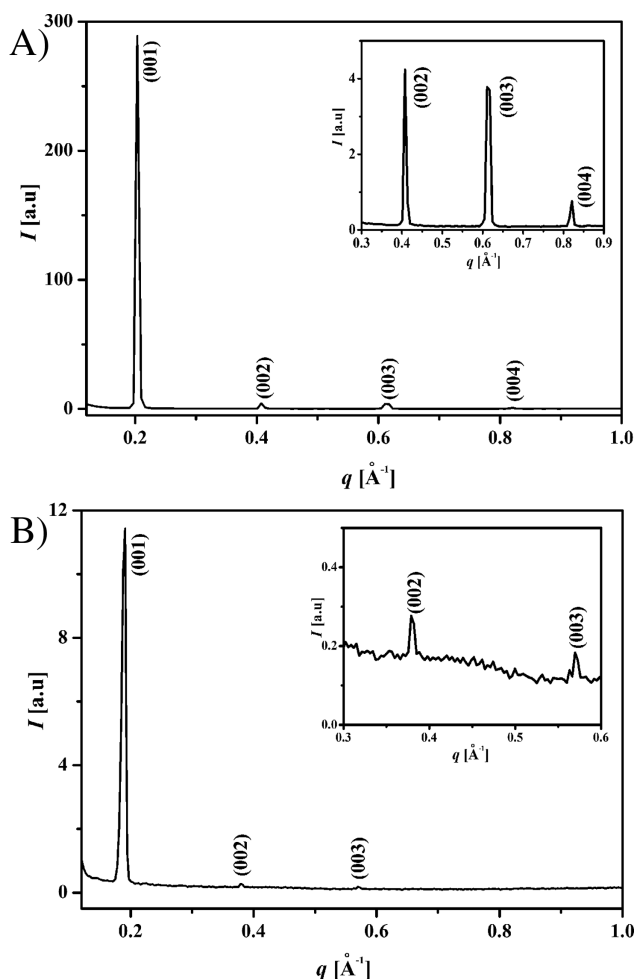


FIGURE 7 Wide-angle X-ray diffraction diagrams corresponding to **G1-(MU)₄** at 100 °C (A) and **G2-(MU)₈** at 70 °C (B).

TABLE 2 X-ray Data for Dendrimers **G1-(MU)₄** and **G2-(MU)₈**

Compound	T (°C)	Phase ^a	$h k l$ ^b	d (Å) ^c
G1-(MU)₄	100	SmA	0 0 1	30.8
			0 0 2	15.4
			0 0 3	10.3
			0 0 4	7.6
G2-(MU)₈	70	SmA	0 0 1	32.9
			0 0 2	16.5
			0 0 3	11.0

^a SmA: smectic-A phase.

^b h, k, l : Miller indices.

^c d : layer spacing.

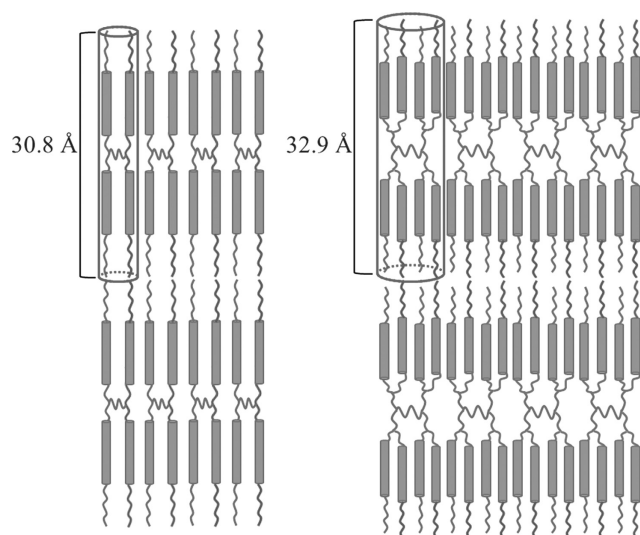


FIGURE 8 Schematic drawing of the proposed molecular packing of dendrimers **G1-(MU)₄** (left) and **G2-(MU)₈** (right).

first- and second-order pseudo-Bragg reflections were associated with a layer thickness of 41.4 Å [Fig. 11(C)]. The angular dispersion of the (001) and (002) reflections is due to the noncomplete orientation of the dendritic molecules during the crosslinking process. In the wide-angle region, two broad diffused peaks partially overlap one another as shown in Figure 11(C). The diffused peak at 4.5 Å corresponds to the lateral distance between aromatic segments and alkyl chains within the layers. Another diffused peak at 8.1 Å is characteristic of interchain packing of siloxane moieties. In contrast with the XRD pattern of **G1-TDS**, **G2-TDS** exhibits only one diffraction arc at low angles [Fig. 11(B)], and the first-order peak ($q = 0.12 \text{ \AA}^{-1}$) indicates a layer period of 52.2 Å [Fig. 11(D)]. Although the superposition of the broad peaks at wide angles becomes obvious, the corresponding distances of the arrangement of alkyl chains and siloxane

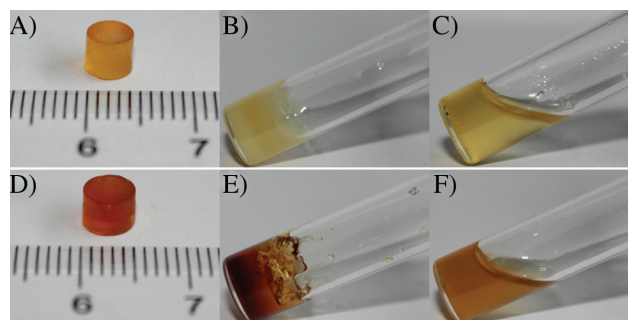


FIGURE 10 Photographs demonstrating the formation of elastomers under different ratio of vinyl group to Si-H bond. **G1-TDS**: (A) 1:1, (B) 2:1, and (C) 4:1. **G2-TDS**: (D) 1:1, (E) 2:1, and (F) 4:1.

moieties remain unchanged. The characteristic distances resulting from the fitting of X-ray pattern are summarized in Table 3. From the 2D-XRD investigation, it is confirmed that the lamellar structure of dendrimers [**G1-(MU)₄** and **G2-(MU)₈**] is actually reserved in the network of elastomers (**G1-TDS** and **G2-TDS**). However, the lamellar spacings of elastomers are greatly enlarged, when compared with those of dendrimers (30.8 and 32.9 Å) formed in their Sma phases. This enlargement can be attributed to the evolution of packing conformation of the dendritic core. After crosslinking reactions, the primary very curled arrangement of dendritic central part was extremely stretched induced by the traction of the siloxane moieties at the crosslinking points.

To evaluate the mechanical properties and response of the two novel elastomers, a cyclic uniaxial compression test that consists of loading (compression) process and unloading (retraction) process was performed. For each sample, four compression cycles were performed, and the stress-strain curves were recorded during the loading process. Figure 12 shows the stress-strain curves of **G1-TDS** and **G2-TDS** under four

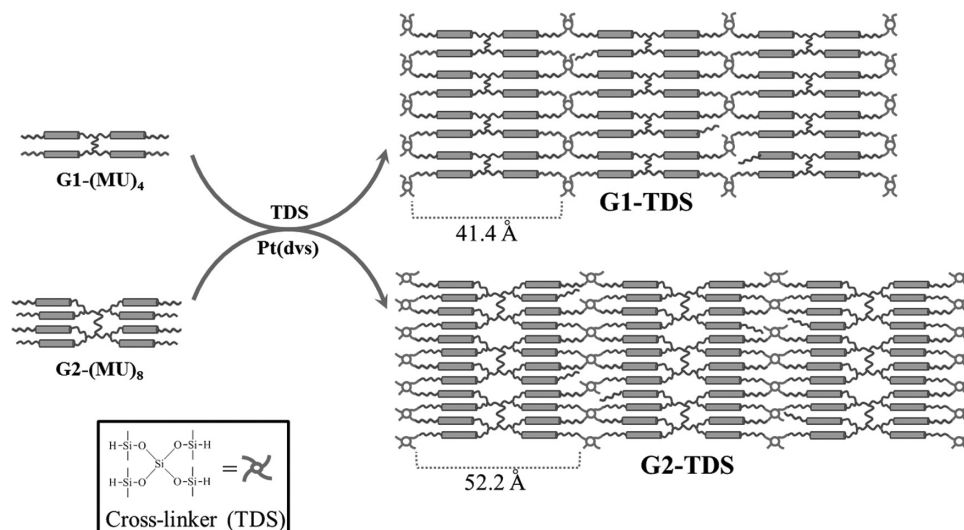


FIGURE 9 Schematic representation of the preparation of elastomers from liquid-crystalline dendrimers.

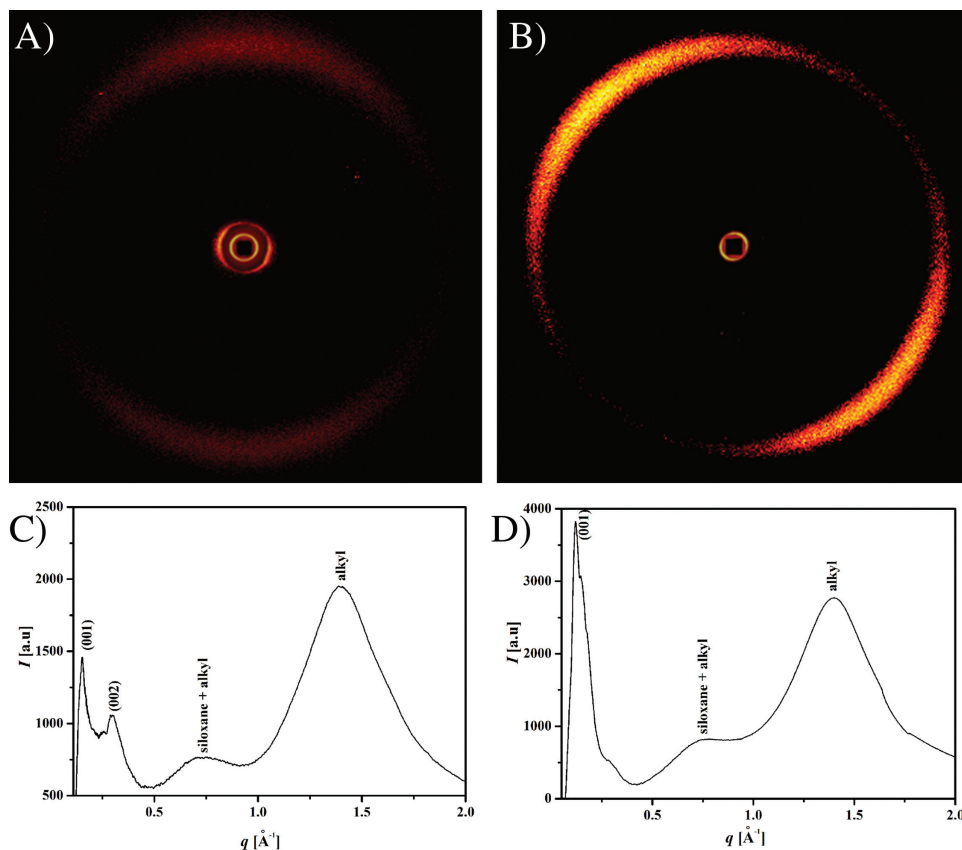


FIGURE 11 Two-dimensional X-ray diffraction pattern of **G1-TDS** (A) and **G2-TDS** (B). Fit of azimuthally integrated X-ray pattern of **G1-TDS** (C) and **G2-TDS** (D) [intensity vs. scattering vector magnitude, $q = 4\pi \sin \theta/\lambda$].

successive uniaxial compressions. In the first compression deformation, the polydomain **G1-TDS** elastomer has a Young's modulus of $E = 2.6$ MPa, which is much smaller than the value for the polydomain **G2-TDS** elastomer ($E = 17.0$ MPa). Moreover, the stress of **G2-TDS** is always higher than that of **G1-TDS** at the same strain, which means that more energy is required to deform the less random distribution of domains of **G2-TDS**. In the crosslinking network of **G2-TDS** (Fig. 9), the mesogens tend to pack closer because of the dendritic monomer **G2-(MU)₈** bearing eight mesogens per molecule. Therefore, a tight lamellar packing and more ordered polydomain form in **G2-TDS** network, in contrast to the loose mesogen packing of **G1-TDS**, is observed. Both **G1-TDS** and **G2-TDS** exhibit excellent recoverability that they can nearly recover their original cylindric shapes (a diameter

of 5 mm and a height of 4 mm) within 1 min after removing of the load. As we can see from Figure 12, the loading curve closely follows the path of the former loading that indicates the elasticity of the two elastomers. Although we measured a full recovery of residual strain after successive compression, an incomplete recovery of the modulus and a stress-

TABLE 3 Fitted Parameters from Azimuthally Integrated X-ray Pattern of **G1-TDS** and **G2-TDS**

Diffraction Peak	Distance (Å) ($2\pi/q$)	
	G1-TDS	G2-TDS
(001)	41.4	52.2
(002)		–
Siloxane moieties	8.1	8.1
Alkyl chains	4.5	4.5

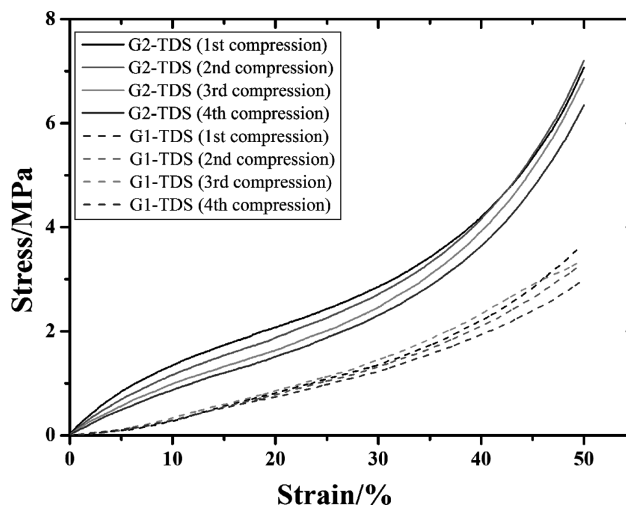


FIGURE 12 Stress–strain curves of elastomers under successive uniaxial compression.

softening phenomenon were observed as mentioned previously by many elastomers.⁶³ In our case, the stress softening may arise from a rearrangement of the elastomer network due to local imbalance in mesogen density and contraction of network chain ends. In particular, uniaxial compressive stress-strain of the polydomain **G2-TDS** revealed three regions^{64,65} with different slopes shown in the true stress-strain curve: (I) $\delta = 0\text{--}6\%$, (II) $\delta = 6\text{--}29\%$, and (III) $\delta = 29\text{--}50\%$. The three regions owning different modulus (E) during deformation of the polydomain elastomer, which might indicate various deformation mechanisms, can be explained by the breakage of the random distribution of the mesogen domains, the rearrangement of those domains, and the protraction of the polymer backbones, respectively.

In both cases of the two elastomers, they are composed of three subsystems: (I) the mesogenic units that self-assemble to give the anisotropic lamellar structures and contribute to the mechanical strength; (II) the dendritic parts between mesogenic units; and (III) the crosslinking area between mesogenic units. The flexibility of subsystems II and III leads to the rubber elasticity of these elastomers. In this novel series of elastomers, although liquid-crystalline phases are not available in contrary to liquid-crystalline elastomers, the combination of anisotropic structures of rigid units and elasticity of flexible networks may make them candidates for the applications in artificial muscles or cartilages.^{66,67} This work represents a proof of the principle that LCDs functionalized with vinyl terminals could be used to develop novel elastomeric materials.

CONCLUSIONS

In summary, we have succeeded in preparing two novel vinyl-terminated side-chain dendrimers by esterification of promesogens and dendritic polyols. The four-armed dendrimer **G1-(MU)₄** and the eight-armed dendrimer **G2-(MU)₈** are able to generate a lamellar SmA mesomorphic phase, indicating that these dendrimers can still display liquid-crystalline phases without the driving force of promoting groups. Competition between anisotropic interactions of terminal mesogenic groups and isotropic distribution of dendritic core is responsible for the self-organization of these compounds in the liquid-crystalline state. Furthermore, the terminal functional vinyl groups of this series of dendrimers make them promising candidates for the construction of liquid-crystalline networks. We innovatively realized the preparation of thermoset elastomers from LCDs by hydrosilylation reaction of vinyl terminals of **G1-(MU)₄** or **G2-(MU)₈** with siloxane crosslinker. Although no mesophase was found in the two elastomers (**G1-TDS** and **G2-TDS**), lamellar packing was able to maintain in the cross-linked network. Moreover, both **G1-TDS** and **G2-TDS** exhibited excellent recoverability after four loading-unloading cycles that indicated their outstanding elasticity.

ACKNOWLEDGMENTS

The authors thank the Shanghai Synchrotron Radiation Facility for providing BL14B1 beamline for collecting synchrotron X-ray powder data.

REFERENCES AND NOTES

- 1 Vögtle, F.; Richardt, G.; Werner, N. *Dendrimer Chemistry*; Wiley-VCH: Weinheim, **2009**.
- 2 Newkome, G. R.; Shreiner, C. *Chem. Rev.* **2010**, *110*, 6338–6442.
- 3 Fréchet, J. M. J.; Tomalia, D. A. *Dendrimers and Other Dendritic Polymers*; Wiley: Chichester, **2001**.
- 4 Newkome, G. R.; Shreiner, C. D. *Polymer* **2008**, *49*, 1–173.
- 5 Astruc, D.; Chardac, F. *Chem. Rev.* **2001**, *101*, 2991–3023.
- 6 Rosen, B. M.; Wilson, C. J.; Wilson, D. A.; Peterca, M.; Imam, M. R.; Percec, V. *Chem. Rev.* **2009**, *109*, 6275–6540.
- 7 Astruc, D.; Boisselier, E.; Ornelas, C. *Chem. Rev.* **2010**, *110*, 1857–1959.
- 8 Jin, G. W.; Koo, H.; Nam, K.; Kim, H.; Lee, S.; Park, J. S.; Lee, Y. *Polymer* **2011**, *52*, 339–346.
- 9 Kono, K.; Fukui, T.; Takagishi, T.; Sakurai, S.; Kojima, C. *Polymer* **2008**, *49*, 2832–2838.
- 10 Ponomarenko, S.; Boiko, N.; Shibaev, V. *Polym. Sci. Ser. C* **2001**, *43*, 1–45.
- 11 Saez, I. M.; Goodby, J. W. *J. Mater. Chem.* **2005**, *15*, 26–40.
- 12 Donnio, B.; Buathong, S.; Bury, I.; Guillon, D. *Chem. Soc. Rev.* **2007**, *36*, 1495–1513.
- 13 Marcos, M.; Martin-Rapun, R.; Omenat, A.; Serrano, J. L. *Chem. Soc. Rev.* **2007**, *36*, 1889–1901.
- 14 Percec, V.; Kawasumi, M. *Macromolecules* **1992**, *25*, 3843–3850.
- 15 Lorenz, K.; Hölter, D.; Stühn, B.; Mülhaupt, R.; Frey, H. *Adv. Mater.* **1996**, *8*, 414–416.
- 16 Baars, M. W. P. L.; Sontjens, S. H. M.; Fischer, H. M.; Peerlings, H. W. I.; Meijer, E. W. *Chem.—Eur. J.* **1998**, *4*, 2456–2466.
- 17 Ponomarenko, S. A.; Boiko, N. I.; Shibaev, V. P.; Richardson, R. M.; Whitehouse, I. J.; Rebrov, E. A.; Muzafarov, A. M. *Macromolecules* **2000**, *33*, 5549–5558.
- 18 Kardas, D.; Prehm, M.; Baumeister, U.; Pocięcha, D.; Reddy, R. A.; Mehl, G. H.; Tschierske, C. *J. Mater. Chem.* **2005**, *15*, 1722–1733.
- 19 Pintre, I. C.; Serrano, J. L.; Ros, M. B.; Martínez-Perdiguero, J.; Alonso, I.; Ortega, J.; Folcia, C. L.; Etxebarria, J.; Alicante, R.; Villacampa, B. *J. Mater. Chem.* **2010**, *20*, 2965–2971.
- 20 García-Frutos, E. M.; Omenat, A.; Barbera, J.; Serrano, J. L.; Gomez-Lor, B. *J. Mater. Chem.* **2011**, *21*, 6831–6836.
- 21 Pastor, L.; Barbera, J.; McKenna, M.; Marcos, M.; Martin-Rapun, R.; Serrano, J. L.; Luckhurst, G. R.; Mainal, A. *Macromolecules* **2004**, *37*, 9386–9394.
- 22 Martin-Rapun, R.; Marcos, M.; Omenat, A.; Serrano, J. L.; Luckhurst, G. R.; Mainal, A. *Chem. Mater.* **2004**, *16*, 4969–4979.
- 23 Barbera, J.; Marcos, M.; Serrano, J. L. *Chem.—Eur. J.* **1999**, *5*, 1834–1840.
- 24 Marcos, M.; Gimenez, R.; Serrano, J. L.; Donnio, B.; Heinrich, B.; Guillon, D. *Chem.—Eur. J.* **2001**, *7*, 1006–1013.
- 25 Barbera, J.; Donnio, B.; Gimenez, R.; Guillon, D.; Marcos, M.; Omenat, A.; Serrano, J. L. *J. Mater. Chem.* **2001**, *11*, 2808–2813.
- 26 Donnio, B.; Barbera, J.; Gimenez, R.; Guillon, D.; Marcos, M.; Serrano, J. L. *Macromolecules* **2002**, *35*, 370–381.
- 27 Rueff, J. M.; Barbera, J.; Donnio, B.; Guillon, D.; Marcos, M.; Serrano, J. L. *Macromolecules* **2003**, *36*, 8368–8375.
- 28 Gehringer, L.; Guillon, D.; Donnio, B. *Macromolecules* **2003**, *36*, 5593–5601.

- 29** Gehringer, L.; Bourgoigne, C.; Guillon, D.; Donnio, B. *J. Am. Chem. Soc.* **2004**, *126*, 3856–3867.
- 30** Gehringer, L.; Bourgoigne, C.; Guillon, D.; Donnio, B. *J. Mater. Chem.* **2005**, *15*, 1696–1703.
- 31** Ungar, G.; Liu, Y. S.; Zeng, X. B.; Percec, V.; Cho, W. D. *Science* **2003**, *299*, 1208–1211.
- 32** Zeng, X. B.; Ungar, G.; Liu, Y. S.; Percec, V.; Dulcey, S. E.; Hobbs, J. K. *Nature* **2004**, *428*, 157–160.
- 33** Percec, V.; Bera, T. K.; Glodde, M.; Fu, Q.; Balagurusamy, V. S. K.; Heiney, P. A. *Chem.—Eur. J.* **2003**, *9*, 921–935.
- 34** Percec, V.; Aqad, E.; Peterca, M.; Imam, M. R.; Glodde, M.; Bera, T. K.; Miura, Y.; Balagurusamy, V. S. K.; Ewbank, P. C.; Würthner, F. *Chem.—Eur. J.* **2007**, *13*, 3330–3345.
- 35** Percec, V.; Glodde, M.; Peterca, M.; Rapp, A.; Schnell, I.; Spiess, H. W.; Bera, T. K.; Miura, Y.; Balagurusamy, V. S. K.; Aqad, E. *Chem.—Eur. J.* **2006**, *12*, 6298–6314.
- 36** Percec, V.; Imam, M. R.; Bera, T. K.; Balagurusamy, V. S. K.; Peterca, M.; Heiney, P. A. *Angew. Chem. Int. Ed. Engl.* **2005**, *44*, 4739–4745.
- 37** Hernández-Ainsa, S.; Barberá, J.; Marcos, M.; Serrano, J. L. *Chem. Mater.*, **2010**, *22*, 4762–4768.
- 38** Hernández-Ainsa, S.; Barberá, J.; Marcos, M.; Serrano, J. L. *J. Polym. Sci. Part A: Polym. Chem.* **2011**, *49*, 278–285.
- 39** Genson, K. L.; Holzmüller, J.; Leshchiner, I.; Agina, E.; Boiko, N.; Shibaev, V. P.; Tsukruk, V. V. *Macromolecules* **2005**, *38*, 8028–8035.
- 40** Baars, M.; Van Boxtel, M.; Bastiaansen, C.; Broer, D.; Söntjens, S.; Meijer, E. *Adv. Mater.* **2000**, *12*, 715–719.
- 41** Burke, K. A.; Mather, P. T. *J. Mater. Chem.* **2010**, *20*, 3449–3457.
- 42** de Jeu, W. H.; Komp, A.; Obratsov, E. P.; Ostrovskii, B. I.; Finkelmann, H. *Soft Matter* **2009**, *5*, 4922–4927.
- 43** Hiraoka, K.; Sagano, W.; Nose, T.; Finkelmann, H. *Macromolecules* **2005**, *38*, 7352–7357.
- 44** Heinze, P.; Finkelmann, H. *Macromolecules* **2010**, *43*, 6655–6665.
- 45** Ohm, C.; Brehmer, M.; Zentel, R. *Adv. Mater.* **2010**, *22*, 3366–3387.
- 46** Donnio, B.; Wermter, H.; Finkelmann, H. *Macromolecules* **2000**, *33*, 7724–7729.
- 47** Rousseau, I. A.; Mather, P. T. *J. Am. Chem. Soc.* **2003**, *125*, 15300–15301.
- 48** Patil, H. P.; Hedden, R. C. *J. Polym. Sci. Part B: Polym. Phys.* **2007**, *45*, 3267–3276.
- 49** Amela-Cortés, M.; Heinrich, B.; Donnio, B.; Evans, K. E.; Smith, C. W.; Bruce, D. W. *J. Mater. Chem.* **2011**, *21*, 8427–8435.
- 50** Marcos, M.; Martín-Rapún, R.; Serrano, J. L.; Sánchez-Ferrer, A. *Macromol. Rapid Commun.* **2005**, *26*, 1604–1608.
- 51** Callau, L.; Reina, J. A.; Mantecón, A. *J. Polym. Sci. Part A: Polym. Chem.* **2002**, *40*, 3893–3908.
- 52** Cai, Z. Q.; Sun, J.; Zhou, Q.; Xu, J. *J. Polym. Sci. Part A: Polym. Chem.* **2007**, *45*, 727–735.
- 53** Hikmet, R.; Lub, J. *Prog. Polym. Sci.* **1996**, *21*, 1165–1209.
- 54** Busson, P.; Ortegren, J.; Ihre, H.; Gedde, U. W.; Hult, A.; Andersson, G.; Eriksson, A.; Lindgren, M. *Macromolecules* **2002**, *35*, 1663–1671.
- 55** Ortegren, J.; Tidlund, J.; Nykvist, M.; Busson, P.; Hult, A.; Sen, S.; Boyd, R. H.; Gedde, U. W. *Polymer* **2001**, *42*, 10027–10033.
- 56** Yonetake, K.; Masuko, T.; Morishita, T.; Suzuki, K.; Ueda, M.; Nagahata, R. *Macromolecules* **1999**, *32*, 6578–6586.
- 57** Corresponding, O. H.; Okuyama, K. I.; Osawa, H.; Yonetake, K. *Liq. Cryst.* **2005**, *32*, 633–642.
- 58** Tokushige, N.; Mihara, T.; Koide, N. *Mol. Cryst. Liq. Cryst.* **2005**, *428*, 33–47.
- 59** Hassner, A.; Alexanian, V. *Tetrahedron Lett.* **1978**, *19*, 4475–4478.
- 60** Lee, G. S.; Lee, Y. J.; Choi, S. Y.; Park, Y. S.; Yoon, K. B. *J. Am. Chem. Soc.* **2000**, *122*, 12151–12157.
- 61** Elemans, J. A. A. W.; Boerakker, M. J.; Holder, S. J.; Rowan, A. E.; Cho, W. D.; Percec, V.; Nolte, R. J. M. *Proc. Natl. Acad. Sci. USA* **2002**, *99*, 5093–5098.
- 62** Vinuales, A. I.; Serrano, J. L.; Gimenez, R.; Pinol, M.; Tomczyk, J.; Stumpe, J. *J. Polym. Sci. Part A: Polym. Chem.* **2011**, *49*, 3499–3512.
- 63** Diani, J.; Fayolle, B.; Gilormini, P. *Eur. Polym. J.* **2009**, *45*, 601–612.
- 64** Amela-Cortés, M.; Bruce, D. W.; Evans, K. E.; Smith, C. W. *J. Mater. Chem.* **2011**, *21*, 8436–8442.
- 65** Sánchez-Ferrer, A.; Finkelmann, H. *Macromol. Rapid Commun.* **2011**, *32*, 309–315.
- 66** Thomsen, D. L., III; Keller, P.; Naciri, J.; Pink, R.; Jeon, H.; Shenoy, D.; Ratna, B. R. *Macromolecules* **2001**, *34*, 5868–5875.
- 67** Webber, R. E.; Creton, C.; Brown, H. R.; Gong, J. P. *Macromolecules* **2007**, *40*, 2919–2927.